



HAL
open science

Characterization of adsorbates by transient measurements in Scanning Electrochemical Microscopy

Dao Trinh, Michel Keddam, Xosé Ramon Novoa, Vincent Vivier

► **To cite this version:**

Dao Trinh, Michel Keddam, Xosé Ramon Novoa, Vincent Vivier. Characterization of adsorbates by transient measurements in Scanning Electrochemical Microscopy. *Electrochimica Acta*, 2014, 131, pp.28-35. 10.1016/j.electacta.2014.02.002 . hal-01020311

HAL Id: hal-01020311

<https://hal.sorbonne-universite.fr/hal-01020311>

Submitted on 18 Jul 2014

HAL is a multi-disciplinary open access archive for the deposit and dissemination of scientific research documents, whether they are published or not. The documents may come from teaching and research institutions in France or abroad, or from public or private research centers.

L'archive ouverte pluridisciplinaire **HAL**, est destinée au dépôt et à la diffusion de documents scientifiques de niveau recherche, publiés ou non, émanant des établissements d'enseignement et de recherche français ou étrangers, des laboratoires publics ou privés.

1
2 **Characterization of adsorbates by**
3 **transient measurements in Scanning**
4 **Electrochemical Microscopy**
5

6 Dao TRINH^{a,b,†,1}, Michel KEDDAM^{a,b}, Xosé Ramón NÓVOA^{c,1},
7 and Vincent VIVIER^{a,b,1,*}
8

9 ^a CNRS, UPR15, Laboratoire Interfaces et Systèmes Electrochimiques, F-75005 Paris,
10 France

11 ^b UPMC Université P. et M. Curie, UPR15, LISE, 4 place Jussieu, F-75005 Paris,
12 France

13 ^c ENCOMAT group, E.E.I, Universidade de Vigo, Campus Universitario, 36310 Vigo,
14 Spain.

15
16
17
18 ¹ ISE member

19 [†] Present address: Université de la Rochelle, Laboratoire des Sciences de l'Ingénieur
20 pour l'Environnement, F-17000 La Rochelle, France

21 * Corresponding author:  vincent.vivier@upmc.fr

22  +33(0)1 4427 4158
23
24

1 **Abstract**

2 In this work, we demonstrate that the use of the scanning electrochemical microscopy in
3 transient mode allows the investigation of adsorbate intermediates at a polarized
4 interface. Two different systems were studied. In the case of a competitive adsorption
5 involving halide and hydrogen, the contribution of each element was monitored
6 independently. Interestingly, the simultaneous measurement of the electrochemical
7 impedance allowed the complex differential capacitance for each adsorbed species to be
8 calculated. In the case of the iron dissolution, the formation of a monovalent Fe species
9 was evidenced allowing to discriminate between different dissolution mechanisms
10 previously described in the literature.

11

12 ***Keywords:*** *Scanning Electrochemical Microscopy; AC-SECM; Adsorbate intermediate;*
13 *Competitive adsorption; Electrochemical impedance spectroscopy.*

14
15

1 **1 Introduction**

2 Electrochemical impedance spectroscopy, EIS, has been widely used for investigating
3 complex electrochemical mechanisms such as those involved in corrosion or metal
4 dissolution [1-5]. When combined with one or more other potential-modulation based
5 techniques, it allows multiple transfer functions to be determined offering the possibility
6 of gathering simultaneously various type of data. For instance, the kinetics and the
7 exchange of ions and molecules inside a thin polymer film has been investigated using
8 ac-electrogravimetry method [6-8], whereas the use of a double-excitation technique
9 allowed the investigation of the double layer relaxation [9-11].

10 It has also been shown that the rotating ring-disk electrode (RRDE) allows the
11 investigation of electrochemical and coupled chemical reactions [12-14]. In their
12 pioneering work, the group of Albery has used the alternating current measurements for
13 defining a complex collection efficiency as the ratio of the ac-current collected at the ring
14 to the ac-current generated at the disk [15-17]. This approach was successfully used for
15 characterizing the formation of thin films at an electrode surface [18, 19], and was
16 extended to channel flow double electrode for the study of the iron dissolution [20].

17 Scanning electrochemical microscopy (SECM) also allows the investigation of the
18 electrochemical interface using a microelectrode as a collecting electrode [21, 22].
19 SECM has been successfully used to investigate intricate systems such as those
20 encountered in corrosion [23-29], for performing the dosing of adsorbed intermediates
21 (electro)generated on a substrate using the surface interrogation mode (SI-SECM) [30-
22 32]. Recently, Trinh et al. [33, 34] have shown that a transient SECM (similarly to what
23 has been done for the RRDE) allowed a quantitative study of adsorption processes.

1 It is generally difficult to identify intermediate species involved in multistep reactions.
2 For instance, halide and hydrogen adsorption have a competitive character [35-37] and
3 various mechanisms involved in corrosion refer to the formation of adsorbates or thin
4 films [1, 2, 19].

5 In this paper, we report on possibility of studying elementary steps by transient SECM.
6 Two different examples are presented: the reduction of proton on a polycrystalline Pt
7 electrode compared with the competitive adsorption of bromide ions and the dissolution
8 of iron in acidic solution. In both cases, the mechanisms are assumed to involve adsorbate
9 intermediates.

10 **2 Experimental**

11 *2.1 Experimental setup*

12 All experiments were performed with a homemade SECM device already described
13 elsewhere [38, 39]. Briefly, it consisted in a 3-axis positioning system (VP-25XA,
14 Newport) driven by a motion encoder (ESP300, Newport) allowing a 3-axis displacement
15 with a 100 nm resolution. The electrochemical measurements were performed with a
16 homemade bi-potentiostat coupled to a low noise current-to-voltage transducer (Femto
17 DLPCA200, BFI Optilas) with adjustable gain (10^3 - 10^{11} V/A). Current and potential
18 measurements were performed with an AD/DA card (PCI-6281 – National Instruments),
19 and the whole experimental device is controlled by a homemade software allowing usual
20 SECM experiment to be achieved, but also multiple transfer functions to be obtained
21 from the different input channels of the data acquisition card. A four-electrode

1 configuration (2 working electrodes, one reference electrode, and one counter electrode)
2 was used as described previously [33, 34].

3 *2.2 Materials and Reagents*

4 Microelectrodes were made from 10 and 40 μm -diameter platinum wires, sealed in a
5 glass capillary by using a microforge. A polycrystalline platinum electrode of 5 mm in
6 diameter isolated by an epoxy resin was used as substrate.

7 All solutions were prepared in distilled water from analytical-grade chemicals. A 0.5 M
8 H_2SO_4 solution was used for the study of the proton reduction and the adsorption of
9 hydrogen on polycrystalline platinum electrode. In order to study the competitive
10 adsorption between hydrogen and bromine on platinum, a mixture of 0.1 M HClO_4 and 5
11 mM KBr was used. Prior to the experiments, Pt electrodes were cleaned by performing
12 repetitive scans over one hour between the HER and the OER reaction in sulfuric acid
13 solution.

14 The iron used in this study was a massive high-purity iron (99.99%) purchased from
15 Johnson-Matthey. It was firstly annealed during 4 h at 995°C in vacuum and then
16 quenched in water. The rod was laterally insulated with a cataphoretic paint and
17 embedded in an epoxy resin. Prior to each experiment, the electrode was polished with
18 SiC paper down to grade 2400, cleaned in water in an ultrasonic bath and then dried with
19 warm air. The anodic dissolution of iron was investigated in 0.5 M H_2SO_4 solution.

20 *2.3 SECM measurements*

21 The dimensionless size of the microelectrode tip RG ($RG = r_g/a$, where r_g is the total
22 external diameter of the microelectrode and a the disc microelectrode radius) and the

1 dimensionless tip-to-substrate distance L ($L = d/a$ where d is the actual tip-to-substrate
2 distance) were determined by performing approach curves in negative feedback mode.
3 The SECM experiments in transient mode and the electrochemical impedance
4 spectroscopy were performed under potentiostatic regulation of the substrate with a
5 50 mV peak-to-peak sine wave perturbation signal. This amplitude was chosen to
6 improve the signal-to-noise ratio, while the linearity condition for the electrochemical
7 system is maintained. The frequency was varied from 10 kHz down to 50 mHz with 7
8 frequencies per decade.

9 **3 Basic of the transient SECM measurements**

10 The transient technique used in this study is based on the former works of Albery et al.
11 [12-14] and Benzekri et al. [18, 19] devised for rotating ring-disk electrode. In
12 generator/collector mode, an obvious analogy exists between the SECM and the RRDE:
13 redox species generated at one electrode can be detected at the second electrode, the time-
14 of-flight being governed by the distance between the probe and the substrate of the
15 SECM experiment, and by the rotation rate and the interelectrode distance in the case of
16 the RRDE. In addition, the collection efficiency can be defined as the ratio of the current
17 of the collecting electrode to that of the generating one. Similar to a usual electrochemical
18 impedance measurement, a small sine-wave perturbation can be superimposed to the dc
19 component of the substrate (at steady-state), allowing the complex transfer function
20 $N(\omega)$ corresponding to the complex collection efficiency to be defined as:

$$21 \quad N(\omega) = \frac{\Delta I_{ip}(\omega)}{\Delta I_{sub}(\omega)} \quad (1)$$

1 where $\Delta I_{tip}(\omega)$ and $\Delta I_{sub}(\omega)$ are the ac-components of the tip and substrate currents,
 2 respectively. The introduction of the electrochemical fluxes at the substrate, $\Delta\Phi_{sub}(\omega)$,
 3 and at the tip, $\Delta\Phi_{tip}(\omega)$, in Eq.(1) allows the rewriting of $N(\omega)$ as:

$$4 \quad N(\omega) = \frac{\Delta I_{tip}(\omega)}{\Delta\Phi_{tip}(\omega)} \cdot \frac{\Delta\Phi_{tip}(\omega)}{\Delta\Phi_{sub}(\omega)} \cdot \frac{\Delta\Phi_{sub}(\omega)}{\Delta I_{sub}(\omega)} \quad (2)$$

5 In the right hand-side of Eq.(2), the first term is the inverse of the complex collection
 6 efficiency on the tip, $N_{tip}(\omega) = \frac{\Delta\Phi_{tip}(\omega)}{\Delta I_{tip}(\omega)}$. For this technique, a simple redox reaction has
 7 to be chosen on the tip (*i.e.* a kinetically fast electrochemical reaction non complicated by
 8 any coupled chemical reaction) in order to maintain its value frequency independent.

9 The second term is the complex transport coefficient, $N_t(\omega) = \frac{\Delta\Phi_{tip}(\omega)}{\Delta\Phi_{sub}(\omega)}$, corresponding
 10 to the mass transport contribution of electroactive species between the substrate and the
 11 tip collector electrode. This contribution always exists and can be determined
 12 experimentally. Fig. 1 shows an example of the Nyquist representation of the complex
 13 collection efficiency measured for a SECM experiment when using ferricyanide as redox
 14 mediator. The potential of the Pt substrate was set at 0.465 V/SHE and the Pt-
 15 microelectrode (tip) was biased at 0.745 V/SHE to oxidize the collected Fe^{2+} species.
 16 When an ac-perturbation was applied to the substrate, the ferrocyanide ions diffuse in
 17 solution and are detected at the tip. The shape of the curve (a semi-cardioid) is very
 18 similar to the curves obtained with the RRDE system [18, 19] or with a channel flow
 19 double electrode system [20]. The low frequency limit corresponds to the steady-state

1 collection efficiency, whereas the high frequency limit was about 100 Hz, which is larger
 2 than with other generator / collector systems and depends on the probe-to-substrate
 3 distance as expected [20]. At higher frequency, the small tail was ascribed to the ohmic
 4 coupling between the two working electrodes as already pointed out for a generator /
 5 collector system by Gabrielli et al. [40]. Thus, the collection response is similar to that of
 6 a low-pass filter [18, 20] and Trinh et al. have also shown that this contribution can be
 7 evaluated numerically by using finite element simulations [33].

8 ----- *Figure 1* -----

9 The last term in the right hand-side of Eq.(2) is the complex emission efficiency of the
 10 substrate, $N_{sub}(\omega) = \frac{\Delta\Phi_{sub}(\omega)}{\Delta I_{sub}(\omega)}$, which is the quantity of interest in this study. It can be
 11 calculated from the independent determination of both the complex collection efficiency
 12 and $N_{sub}(\omega)$. Further, if the double-layer charging is neglected, the non-steady-state
 13 current measured at the substrate is the sum of the flux of species released in solution,
 14 $\Delta\Phi_{sub}$, and of the Faradaic charge stored at the interface, ΔQ_{sub} , corresponding to the
 15 formation of adsorbate intermediates or thin solid films:

$$16 \quad \Delta I_{sub} = n_{sub} F \Delta\Phi_{sub} + \frac{d\Delta Q_{sub}}{dt} \quad (3)$$

17 where n_{sub} is the number of electrons involved in the electrochemical reaction at the
 18 substrate, and F the Faraday constant. In the frequency domain, Eq.(3) can be rewritten in
 19 dimensionless form as:

$$20 \quad n_{sub} F N_{sub} + j\omega \frac{\Delta Q_{sub}(\omega)}{\Delta I_{sub}(\omega)} = 1 \quad (4)$$

1 In a Nyquist representation Eq.(4) corresponds to a semi circle in which $j\omega \frac{\Delta Q_{sub}(\omega)}{\Delta I_{sub}(\omega)}$ is
2 the contribution of the charge exchanged for the formation of the adsorbates at the
3 substrate. The high frequency limit of Eq.(4) corresponds to the kinetics of processes
4 taking place at the substrate when controlled by the charge transfer resistance.
5 Conversely, at the low frequency limit, the right hand-side term is null and the steady-
6 state requires that the flux and the current are linked through the Faraday constant.

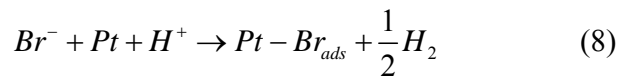
7 The experimental setup used in this work allows the simultaneous measurement of the
8 complex collection efficiency and the electrochemical impedance of the substrate,
9 $Z_{sub}(\omega)$. Thus from Eq.(4), the differential capacitance of the substrate, C_d , can be then
10 calculated as:

$$11 \quad C_d(\omega) = \frac{\Delta Q_{sub}(\omega)}{\Delta E_{sub}(\omega)} = \frac{1 - n_{sub} F \Delta N_{sub}(\omega)}{j\omega Z_{sub}(\omega)} \quad (5)$$

12 This provides a unique way of determining the relaxation ascribed to the charge stored at
13 the interface during the electrochemical process.

14 In the following section, this new technique will be used for the study of competitive
15 adsorption between hydrogen and bromide ions on a Pt substrate and for the dissolution
16 mechanism of iron.

1 in a solution of HClO₄. They showed that the presence of bromide significantly alters the
2 adsorption of hydrogen that was attributed to the competitive adsorption of bromine
3 through the following reaction:



5 The presence of bromide significantly alters the adsorption of hydrogen resulting in the
6 gradual disappearance of the adsorption/desorption peak at about 0.260 V/SHE.
7 Concomitantly, the peak at 0.135 V/SHE increases with the bromide ion concentration,
8 which confirms the competitive adsorption of bromine and hydrogen.

9 In this case, the total exchanged charge involved through the competitive formation of the
10 hydrogen and bromine adsorbed layer is the sum of the charge required for the adsorption
11 of each species, ΔQ_{sub}^H and ΔQ_{sub}^{Br} , respectively.

$$12 \quad \Delta Q_{sub} = \Delta Q_{sub}^H + \Delta Q_{sub}^{Br} \quad (9)$$

13 The potential corresponding to the adsorption reaction of bromine is very close to the
14 adsorption potential of hydrogen and it is difficult to distinguish between these two
15 phenomena by conventional electrochemical methods, especially on a single
16 voltammogram. By performing the transient SECM measurements while detecting
17 different species generated from the substrate, specific information about each adsorption
18 process can be gathered and the competitive reaction between the adsorption of bromine
19 and hydrogen can be selectively studied.

1 Figure 4 shows the differential capacitance $\frac{\Delta Q_{sub}}{\Delta E_{sub}}$ calculated from the experimental
 2 complex collection efficiency according to Eq. (5) in the case of bromine and hydrogen
 3 adsorption. The transient SECM measurements were performed at $E_{sub} = 1.19$ V/SHE for
 4 bromine and $E_{sub} = -0.005$ V/SHE for hydrogen. For electrode potential value lower than
 5 -0.005 V/SHE, the HER occurs on the substrate to form dissolved hydrogen which is then
 6 captured and oxidized by the tip (the tip is biased at 0.645 V/SHE). This reaction involves
 7 adsorbed intermediate according to the Volmer – Tafel or Volmer – Heyrovsky
 8 mechanism.

9 ----- Figure 4 -----

10 At 1.19 V/SHE, Br^- is oxidized to Br_2 (Br_3^-) which is then detected at the tip (tip potential
 11 is maintained at 0.645 V/SHE to reduce the Br_2 generated at the substrate). In both cases,
 12 the HF limit tends towards 0 because in the frequency domain, the impedance is governed
 13 purely by the charge transfer resistance. The low frequency limit corresponds to the
 14 charge accumulation at the electrode surface, *i.e.*, 1 mFcm⁻² for hydrogen and 1.2 mF
 15 mFcm⁻² for bromine (Table 1). The latter value corresponds to the accumulation of
 16 charge on the substrate associated with the competitive adsorption between H_{ads} and
 17 Br_{ads} .

18 ----- Table 1 -----

19 Thus, varying the electrode potential allows the different contribution of adsorbed species
 20 to be evaluated and the sum of charges involved in the formation of H_{ads} and Br_{ads} is
 21 given by $\Delta Q_{sub} = \Delta Q_{sub}^H + \Delta Q_{sub}^{Br} = 71 + 85 = 156 \mu C cm^{-2}$. This value (156 $\mu C cm^{-2}$) is

1 smaller than the one obtained for a monolayer of adsorbed hydrogen in the absence of
2 bromide ions ($212 \mu\text{C cm}^{-2}$) which confirms the hypothesis of competitive adsorption of
3 bromide ions on the site occupied by hydrogen on platinum substrate. It should also be
4 mentioned that because both electrodes (tip and substrate) are made from the same
5 material and were prepared following the same experimental procedure (grinding,
6 washing, electrochemical cleaning), the roughness factor for each electrode was assumed
7 to be the same. This allows expecting that the complex collection efficiency to be
8 independent of this roughness factor.

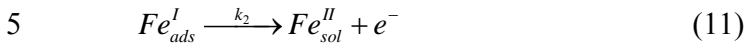
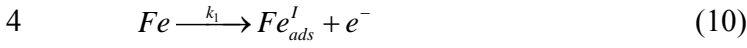
9 In addition, the time-constant for the relaxation of H_{ads} at the electrode surface without
10 the bromide ion in solution is about 2 Hz [34]. This frequency points to a kinetics ten
11 times faster than the value determined in presence of bromide ions (Figure 4). All the
12 characteristic constants extracted from these experiments are reported in Table 1. This
13 behavior indicates a change in the mechanism and kinetics of adsorption of hydrogen in
14 presence of a competitive adsorption.

15 *4.2 Mechanism of iron dissolution in acidic solution*

16 The dissolution mechanism of iron in an acidic solution has been the topic of controversy
17 [44]. Two different mechanisms were considered based on the interpretation of current
18 potential curves and electrochemical impedance diagrams [44-46], in which adsorbed
19 monovalent iron species act as an intermediate in the transfer of the first and second
20 electrons of Fe (mechanism proposed by J. O'M. Bockris, et al. [45]) whereas Heusler
21 [46] suggested that it acts as a catalyst in the dissolution of divalent Fe cations in acidic
22 solutions.

1 These two mechanisms can be summarized as follows:

2 Bockris' mechanism [45] is described by two successive and irreversible elementary
3 steps involving Fe_{ads}^I as adsorbate intermediate:



6 Thus, mass and charge balances can be expressed as

$$7 \quad \beta \frac{d\theta}{dt} = k_1(1-\theta) - k_2\theta \quad (12)$$

$$8 \quad i_{sub} = F(k_1(1-\theta) + k_2\theta) \quad (13)$$

9 where θ is the fractional surface coverage of Fe_{ads}^I and β is the maximum of surface
10 concentration of adsorbate intermediate. The flux of electrogenerated species at the
11 substrate is then given by

$$12 \quad \Phi_{sub} = k_2\theta \quad (14)$$

13 At steady-state, the fractional surface coverage is given by

$$14 \quad \bar{\theta} = \frac{k_1}{k_1 + k_2} \quad (15)$$

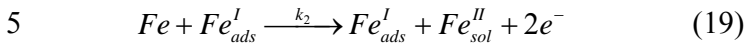
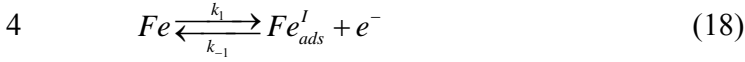
15 The impedance of the substrate is given by

$$16 \quad \frac{1}{Z_{sub}} = F \left[(b_1 + b_2)k_2\bar{\theta} - (k_1 - k_2) \frac{(b_1 - b_2)k_2\bar{\theta}}{k_1 + k_2 + \beta j\omega} \right] \quad (16)$$

17 allowing the collection efficiency to be calculated as

$$N_{sub} = \left(b_2 k_2 \bar{\theta} + k_2 \frac{(b_1 - b_2) k_2 \bar{\theta}}{k_1 + k_2 + \beta j \omega} \right) \times Z_{sub} \quad (17)$$

The mechanism proposed by Heusler [46] also involves Fe_{ads}^I as adsorbate intermediate, but the later acts as a catalyst:



The mass and charge balances can then be expressed as

$$\beta \frac{d\theta}{dt} = k_1 (1 - \theta) - k_{-1} \theta \quad (20)$$

$$i_{sub} = F (k_1 (1 - \theta) - k_{-1} \theta + 2k_2 \theta) \quad (21)$$

The flux of electrogenerated species at the substrate is also given by

$$\Phi_{sub} = k_2 \theta \quad (22)$$

At steady-state, the fractional surface coverage is given by

$$\bar{\theta} = \frac{k_1}{k_1 + k_{-1}} \quad (23)$$

The impedance of the substrate is given by

$$\frac{1}{Z_{sub}} = F \left[(b_1 - b_{-1}) k_{-1} \bar{\theta} + 2k_2 b_2 \bar{\theta} - (k_1 + k_{-1} - 2k_2) \frac{k_{-1} (b_1 - b_{-1}) \bar{\theta}}{k_1 + k_{-1} + \beta j \omega} \right] \quad (24)$$

allowing the collection efficiency to be calculated as

$$N_{sub} = \left(b_2 k_2 \bar{\theta} + k_2 \frac{k_{-1} (b_1 - b_{-1}) \bar{\theta}}{k_1 + k_{-1} + \beta j \omega} \right) \times Z_{sub} \quad (25)$$

----- Figure 5 -----

Fig. 5 shows the experimental impedance diagrams measured at the onset of the dissolution peak of pure iron as a function of the electrode potential. In each case two loops are evidenced, a high frequency capacitive one corresponding to the double layer capacity-charge transfer resistance and a low frequency inductive one generated by the frequency response of the surface coverage by the adsorbed reaction intermediate. These diagrams are characterized by a decrease of the impedance (larger value of the dissolution current) and a shift of the characteristic frequency towards shorter time-constant as the potential increases for both loops. Assuming that electrochemical steps follow Tafel kinetics and using the linearized expression of the currents given by Eq.(13) and Eq.(21), it is possible to calculate the impedance response as shown in Fig. 6a for the Bockris' mechanism and Fig. 6b Heusler's mechanism. Independently of the kinetic constants used for the simulation, in both cases the shape of the impedance diagrams are very similar to those obtained experimentally. Both the amplitude and time-constants vary in the same way. It is thus difficult to decide which mechanism is the most suited.

----- Figure 6 -----

----- Figure 7 -----

Fig. 7 shows the calculated collection efficiency of the substrate using the same set of parameters as those used for the impedance diagrams presented in Fig. 6. Interestingly, a

1 different behavior is observed. In the case of Bockris' mechanism, the collection
2 efficiency locus overlap in amplitude and a small frequency shift can be observed (Fig.
3 7a) whereas for Heusler's mechanism, the amplitude of the complex collection efficiency
4 is potential dependent (Fig. 7b). As the potential increases, the high frequency limit
5 increases corresponding to a change of the kinetic process at the substrate under the
6 assumption of vanishing variations of the superficial concentration.

7 ----- *Figure 8* -----

8 Fig. 8 shows the experimental complex collection efficiency of the substrate measured
9 simultaneously with the impedance diagrams presented in Fig. 5. The shape of the
10 transfer function does not depend on the potential and a small frequency shift is observed.
11 These results compare favorably with the theoretical curves presented in Fig. 7a
12 indicating that the Bockris' mechanism allows a quantitative description of the iron
13 dissolution valid at low current densities and low pH [1, 2]. Thus the transient SECM
14 allows distinguishing between different possible mechanisms. It should be mentioned that
15 for experiments performed at higher potentials (thus for larger steady-state dissolution
16 current), no reliable results could have been obtained. This was ascribed to the fact that
17 under high dissolution rates the distance between the Pt-probe and the iron substrate
18 varies too quickly compared to the time-scale of the impedance acquisition rate.

19 **5 Conclusions**

20 In this work, we have highlighted different intakes that can be obtained using the SECM
21 in transient mode in order to characterize an electrified interface.

1 In the case of competitive adsorption between halide ions and hydrogen, it was shown
2 that it is possible to discriminate between the different species and to evaluate
3 independently the charge exchanged for each adsorbate.

4 In the case of the formation of an adsorbate intermediates like Fe(I) species, the complex
5 collection efficiency of the substrate can decide between different mechanisms and
6 appears to be a complementary approach to the usual impedance measurements.

7 The perspectives of this work are the investigation of reaction mechanism on well
8 oriented materials such as the absorption and the competitive adsorption on single
9 crystals and the investigation of the passive film formation and passive film reactivity as
10 a function of the grain orientation.

11 **Acknowledgements**

12 The authors gratefully acknowledge D. Rose (UPR15) for technical support.

13

1

2 **References**

3 [1] M. Keddam, O.R. Mattos, H. Takenouti, Reaction model for iron dissolution studied
4 by electrode impedance. II. Determination of the reaction model, *J. Electrochem. Soc.*,
5 128 (1981) 266-274.

6 [2] M. Keddam, O.R. Mattos, H. Takenouti, Reaction model for iron dissolution studied
7 by electrode impedance. I. Experimental results and reaction model, *J. Electrochem. Soc.*,
8 128 (1981) 257-266.

9 [3] I. Epelboin, C. Gabrielli, M. Keddam, H. Takenouti, Model of the anodic behavior of
10 iron in sulfuric acid medium, *Electrochim. Acta*, 20 (1975) 913-916.

11 [4] C. Cachet, F. Ganne, G. Maurin, J. Petitjean, V. Vivier, R. Wiart, EIS investigation of
12 zinc dissolution in aerated sulfate medium. Part I: bulk zinc, *Electrochim. Acta*, 47 (2001)
13 509-518.

14 [5] C. Cachet, F. Ganne, S. Joiret, G. Maurin, J. Petitjean, V. Vivier, R. Wiart, EIS
15 investigation of zinc dissolution in aerated sulphate medium. Part II: zinc coatings,
16 *Electrochim. Acta*, 47 (2002) 3409-3422.

17 [6] C. Gabrielli, M. Keddam, N. Nadi, H. Perrot, a.c. Electrogravimetry on conducting
18 polymers. Application to polyaniline, *Electrochim. Acta*, 44 (1999) 2095-2103.

19 [7] J. Agrisuelas, C. Gabrielli, J.J. García-Jareño, H. Perrot, F. Vicente, Kinetic and
20 Mechanistic Aspects of a Poly(o-Toluidine)-Modified Gold Electrode. 2. Alternating
21 Current Electrogravimetry Study in H₂SO₄ Solutions, *J. Phys. Chem. C*, 116 (2012)
22 15630-15640.

- 1 [8] T.K.L. To, C. Debiemme-Chouvy, C. Gabrielli, H. Perrot, Redox Switching of
2 Heteropolyanions Entrapped in Polypyrrole Films Investigated by ac Electrogravimetry,
3 *Langmuir*, 28 (2012) 13746-13757.
- 4 [9] R. Antano-Lopez, M. Keddad, H. Takenouti, A new experimental approach to the
5 time-constants of electrochemical impedance: frequency response of the double layer
6 capacitance, *Electrochim. Acta*, 46 (2001) 3611-3617.
- 7 [10] R. Antano-Lopez, M. Keddad, H. Takenouti, Interface capacitance at mercury and
8 iron electrodes in the presence of organic compound, *Corros. Eng., Sci. Technol.*, 39
9 (2004) 59-64.
- 10 [11] E.R. Larios-Duran, R. Antano-Lopez, M. Keddad, Y. Meas, H. Takenouti, V.
11 Vivier, Dynamics of double-layer by AC Modulation of the Interfacial Capacitance and
12 Associated Transfer Functions, *Electrochim. Acta*, 55 (2010) 6292-6298.
- 13 [12] W.J. Albery, S. Bruckenstein, Ring-disk electrodes. VII. Homogeneous and
14 heterogeneous kinetics, *Trans. Faraday Soc.*, 62 (1966) 2596-2606.
- 15 [13] W.J. Albery, S. Bruckenstein, Ring-disk electrodes. V. First-order kinetic collection
16 efficiencies at the ring electrode, *Trans. Faraday Soc.*, 62 (1966) 1946-1954.
- 17 [14] W.J. Albery, S. Bruckenstein, Ring-disk electrodes. II. Theoretical and experimental
18 collection efficiencies, *Trans. Faraday Soc.*, 62 (1966) 1920-1931.
- 19 [15] S. Bruckenstein, K. Tokuda, W.J. Albery, Ring-disk electrodes. Part 17. Ring
20 response to periodic disk electrode forcing functions, *J. Chem. Soc, Farad. T. 1*, 73
21 (1977) 823-829.
- 22 [16] W.J. Albery, R.G. Compton, A.R. Hillman, Ring-disk electrodes. Part 18. Collection
23 efficiency for high frequency a.c, *J. Chem. Soc, Farad. T. 1*, 74 (1978) 1007-1019.

- 1 [17] W.J. Albery, A.R. Hillman, Ring-disk electrodes. Part 19. Adsorption studies at low
2 frequency a.c, J. Chem. Soc, Farad. T. 1, 75 (1979) 1623-1634.
- 3 [18] N. Benzekri, M. Keddou, H. Takenouti, The a.c. response of a rotating ring-disk
4 electrode: application to 2-D and 3-D film formation in anodic processes, *Electrochim.*
5 *Acta*, 34 (1989) 1159-1166.
- 6 [19] N. Benzekri, R. Carranza, M. Keddou, H. Takenouti, The a.c. response of RRDE
7 during the passivation of iron, *Corros. Sci.*, 31 (1990) 627-635.
- 8 [20] M. Itagaki, M. Tagaki, K. Watanabe, Active dissolution mechanisms of iron using
9 EIS with channel flow double electrode. Influences of chloride and fluoride ions,
10 *Electrochim. Acta*, 41 (1996) 1201-1207.
- 11 [21] G. Wittstock, M. Burchardt, S.E. Pust, Y. Shen, C. Zhao, Scanning electrochemical
12 microscopy for direct imaging of reaction rates, *Angew. Chem. Int. Ed.*, 46 (2007) 1584-
13 1617.
- 14 [22] S. Amemiya, A.J. Bard, F.R.F. Fan, M.V. Mirkin, P.R. Unwin, Scanning
15 Electrochemical Microscopy, in: *Annual Review of Analytical Chemistry*, vol. 1, 2008,
16 pp. 95-131.
- 17 [23] M.B. Jensen, D.E. Tallman, Application of SECM to corrosion studies, *Electroanal.*
18 *Chem.*, 24 (2012) 171-286.
- 19 [24] N. Casillas, S.J. Charlebois, W.H. Smyrl, H.S. White, Scanning electrochemical
20 microscopy of precursor sites for pitting corrosion on titanium, *J. Electrochem. Soc.*, 140
21 (1993) L142-L145.
- 22 [25] N. Casillas, S. Charlebois, W.H. Smyrl, H.S. White, Pitting Corrosion of Titanium,
23 *J. Electrochem. Soc.*, 141 (1994) 636-642.

- 1 [26] M.B. Jensen, A. Guerard, D.E. Tallman, G.P. Bierwagen, Studies of electron transfer
2 at aluminum alloy surfaces by scanning electrochemical microscopy, *J. Electrochem.*
3 *Soc.*, 155 (2008) C324-C332.
- 4 [27] C. Gabrielli, S. Joiret, M. Keddam, H. Perrot, N. Portail, P. Rousseau, V. Vivier,
5 Development of a Coupled SECM-EQCM Technique for the Study of Pitting Corrosion
6 on Iron, *J. Electrochem. Soc.*, 153 (2006) B68-B74.
- 7 [28] C. Gabrielli, S. Joiret, M. Keddam, H. Perrot, N. Portail, P. Rousseau, V. Vivier, A
8 SECM assisted EQCM study of iron pitting, *Electrochim. Acta*, 52 (2007) 7706-7714.
- 9 [29] C. Gabrielli, S. Joiret, M. Keddam, N. Portail, P. Rousseau, V. Vivier, Single pit on
10 iron generated by SECM, *Electrochim. Acta*, 53 (2008) 7539-7548.
- 11 [30] J. Rodriguez-Lopez, M.A. Alpuche-Aviles, A.J. Bard, Interrogation of Surfaces for
12 the Quantification of Adsorbed Species on Electrodes: Oxygen on Gold and Platinum in
13 Neutral Media, *J. Am. Chem. Soc.*, 130 (2008) 16985-16995.
- 14 [31] Q. Wang, J. Rodriguez-Lopez, A.J. Bard, Reaction of Br₂ with Adsorbed CO on Pt,
15 Studied by the Surface Interrogation Mode of Scanning Electrochemical Microscopy, *J.*
16 *Am. Chem. Soc.*, 131 (2009) 17046-17047.
- 17 [32] J. Rodriguez-Lopez, A. Minguzzi, A.J. Bard, Reaction of various reductants with
18 oxide films on Pt electrodes as studied by the surface interrogation mode of scanning
19 electrochemical microscopy (SI-SECM): Possible validity of a Marcus relationship, *J.*
20 *Phys. Chem. C*, 114 (2010) 18645-18655.
- 21 [33] D. Trinh, M. Keddam, X.R. Nova, V. Vivier, Alternating-Current Measurements in
22 Scanning Electrochemical Microscopy, Part 1: Principle and Theory, *ChemPhysChem*,
23 12 (2011) 2169-2176.

- 1 [34] D. Trinh, M. Keddad, X.R. Novoa, V. Vivier, Alternating Current Measurements in
2 Scanning Electrochemical Microscopy, Part 2: Detection of Adsorbates,
3 ChemPhysChem, 12 (2011) 2177-2183.
- 4 [35] N. Garcia-Araez, V. Climent, E. Herrero, J.M. Feliu, On the electrochemical
5 behavior of the Pt(100) vicinal surfaces in bromide solutions, Surf. Sci., 560 (2004) 269-
6 284.
- 7 [36] N. Garcia-Araez, V. Climent, E. Herrero, J. Feliu, J. Lipkowski, Thermodynamic
8 studies of chloride adsorption at the Pt(111) electrode surface from 0.1 M HClO₄
9 Solution, J. Electroanal. Chem., 576 (2005) 33-41.
- 10 [37] N. Garcia-Araez, J.J. Lukkien, M.T.M. Koper, J.M. Feliu, Competitive adsorption of
11 hydrogen and bromide on Pt(100): Mean-field approximation vs. Monte Carlo
12 simulations, J. Electroanal. Chem., 588 (2006) 1-14.
- 13 [38] C. Gabrielli, E. Ostermann, H. Perrot, V. Vivier, L. Beitone, C. Mace, Concentration
14 mapping around copper microelectrodes studied by scanning electrochemical
15 microscopy, Electrochem. Commun., 7 (2005) 962-968.
- 16 [39] C. Gabrielli, M. Keddad, N. Portail, P. Rousseau, H. Takenouti, V. Vivier,
17 Electrochemical Impedance Spectroscopy Investigations of a Microelectrode Behavior in
18 a Thin-Layer Cell: Experimental and Theoretical Studies, J. Phys. Chem. B, 110 (2006)
19 20478-20485.
- 20 [40] C. Gabrielli, M. Keddad, H. Takenouti, Potential distribution at the surface of a
21 ring-disk electrode, J. Chim. Phys. PCB, 69 (1972) 737-740.
- 22 [41] S. Ferro, A. De Battisti, The Bromine Electrode. Part I: Adsorption Phenomena at
23 Polycrystalline Platinum Electrodes, J. Appl. Electrochem., 34 (2004) 981-987.

- 1 [42] G.N. Salaita, D.A. Stern, F. Lu, H. Baltruschat, B.C. Schardt, J.L. Stickney, M.P.
2 Soriaga, D.G. Frank, A.T. Hubbard, Structure and composition of a Platinum(111)
3 surface as a function of pH and electrode potential in aqueous bromide solutions,
4 *Langmuir*, 2 (1986) 828-835.
- 5 [43] S. Ferro, C. Orsan, A. De Battisti, The bromine electrode Part II: reaction kinetics at
6 polycrystalline Pt, *J. Appl. Electrochem.*, 35 (2005) 273-278.
- 7 [44] M. Keddam, H. Takenouti, Mechanism of anodic dissolution of iron in acid solution,
8 *CR Acad. Sci. II C*, 270 (1970) 283-286.
- 9 [45] J.O.M. Bockris, D. Drazic, A.R. Despic, The electrode kinetics of the deposition and
10 dissolution of iron, *Electrochim. Acta*, 4 (1961) 325-361.
- 11 [46] K.E. Heusler, Der Einfluß der Wasserstoff Ionenkonzentration auf das
12 elektrochemische Verhalten des aktiven Eisens in sauren Lösungen, *Z. Elektrochem.*, 62
13 (1958) 582-587.

14

15

Figure captions

Figure 1: Complex experimental collection efficiency for a 50 mM $\text{Fe}(\text{CN})_6^{3-}$ + 0.5 M KCl solution with the tip-to-substrate distance as a parameter. The tip was a Pt microelectrode, 20 μm in diameter, biased at 0.745 V/SHE and the Pt substrate at 0.465 V/SHE

Figure 2: Schematic representation of a monolayer of hydrogen adsorbed on platinum (a) and the competitive adsorption between hydrogen and bromine on platinum (b).

Figure 3: Cyclic voltammogram of the polycrystalline platinum electrode (0.5 cm in diameter) in a 5 mM KBr + 0.1 M HClO_4 solution – initial potential 0.445 V/SHE – 5 cycles at 50 mVs^{-1} .

Figure 4: Differential capacitances calculated from the complex experimental collection efficiency according to Eq. (5) $E_{sub} = -0.005$ V/SHE, Pt-tip: 20 μm in radius, Pt-substrate 0.5 cm diameter. Solution: 0.1 M HClO_4 + 5 mM KBr.

Figure 5: Electrochemical impedance diagrams of pure iron in sulfuric acid solution (0.5 M) as a function of the electrode potential.

Figure 6: Simulated electrochemical impedance diagrams for pure iron in sulfuric acid solution as a function of the electrode potential using Refs. [1, 2] for the choice of kinetic constants. (a) Bockris' mechanism: $k_1 = 0.4 \cdot 10^6 e^{b_1 \cdot E}$; $b_1 = 38.4 \text{ V}^{-1}$; $k_2 = 8 \cdot 10^{-4} e^{b_2 \cdot E}$; $b_2 = 7 \text{ V}^{-1}$; $\beta = 10^{-8} \text{ mol} \cdot \text{cm}^{-2}$; $C_d = 100 \mu\text{F}$ (b) Heusler's mechanism: $k_1 = 10 e^{b_1 \cdot E}$;

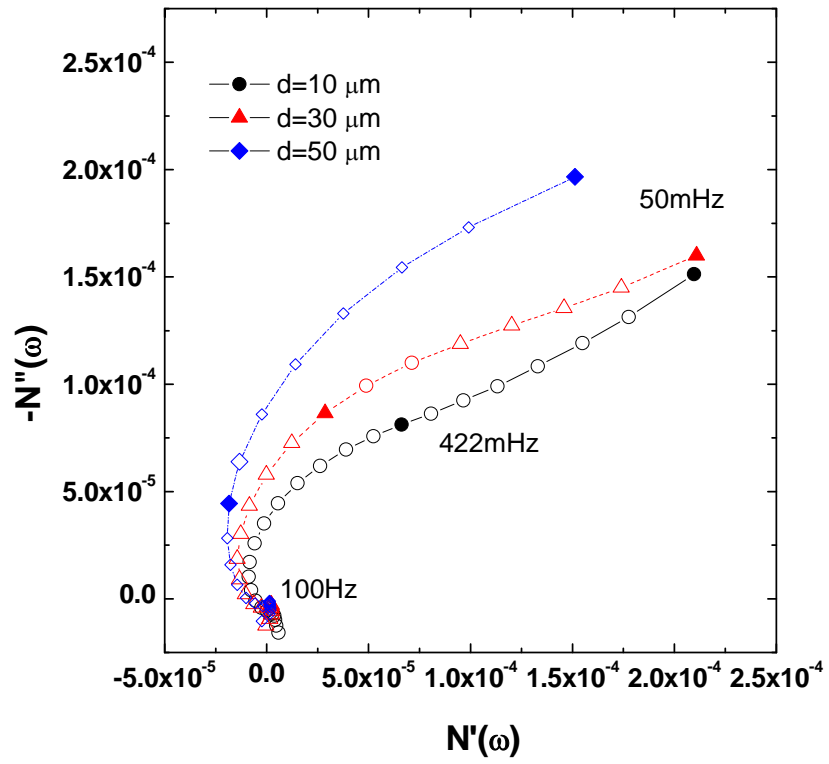
1 $b_1 = 19.2 \text{ V}^{-1}; \quad k_{-1} = 15 \cdot 10^{-18} e^{-b_{-1} \cdot E}; \quad b_{-1} = 19.2 \text{ V}^{-1}; k_2 = 8 \cdot 10^{-4} e^{b_2 \cdot E}; \quad b_2 = 7 \text{ V}^{-1};$
2 $\beta = 10^{-8} \text{ mol} \cdot \text{cm}^{-2}; C_d = 100 \text{ } \mu\text{F}.$

3 **Figure 7:** Simulated collection efficiency of the substrate for pure iron in sulfuric acid
4 solution as a function of the electrode potential (same kinetic constants as in Fig. 6). (a)
5 Bockris' mechanism, (b) Heusler's mechanism.

6 **Figure 8:** Experimental collection efficiency of the substrate for pure iron in sulfuric acid
7 solution (0.5 M) as a function of the electrode potential.

8
9 **Table 1:** Capacitance, charge and time constant of the adsorption processes for the
10 different experiments performed.

1 *Figure 1*



2

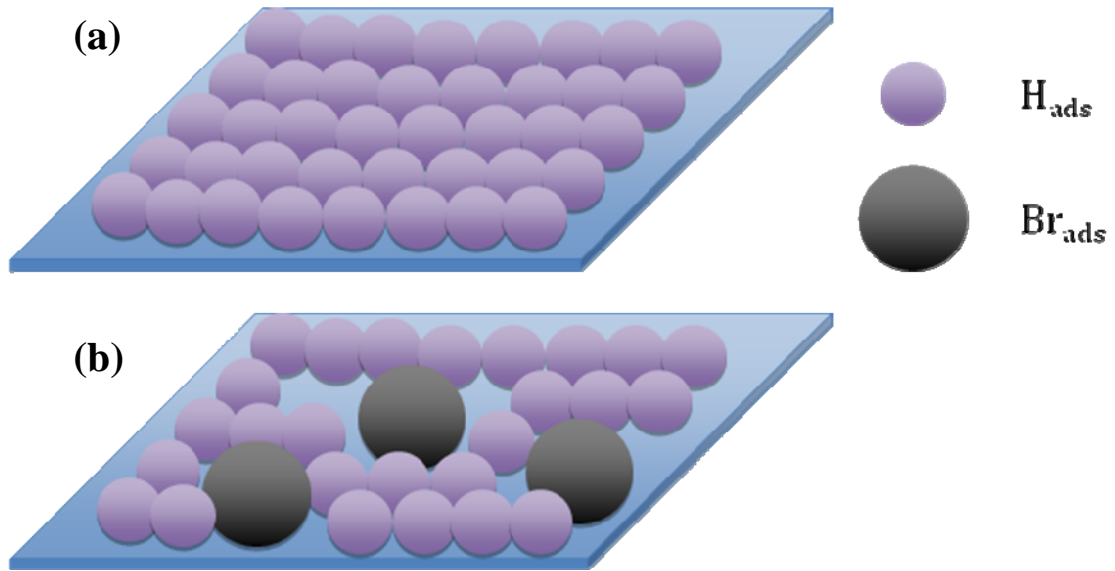
3

4

1
2

Figure 2

3



4

5

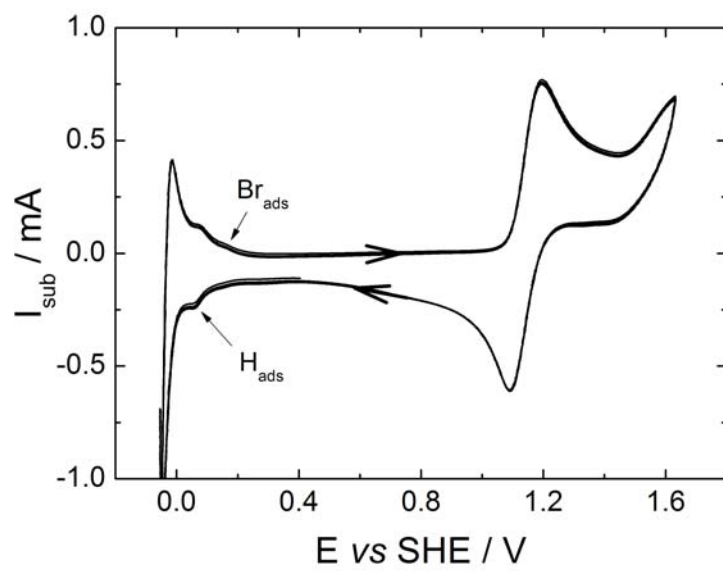
6

7

8

1
2

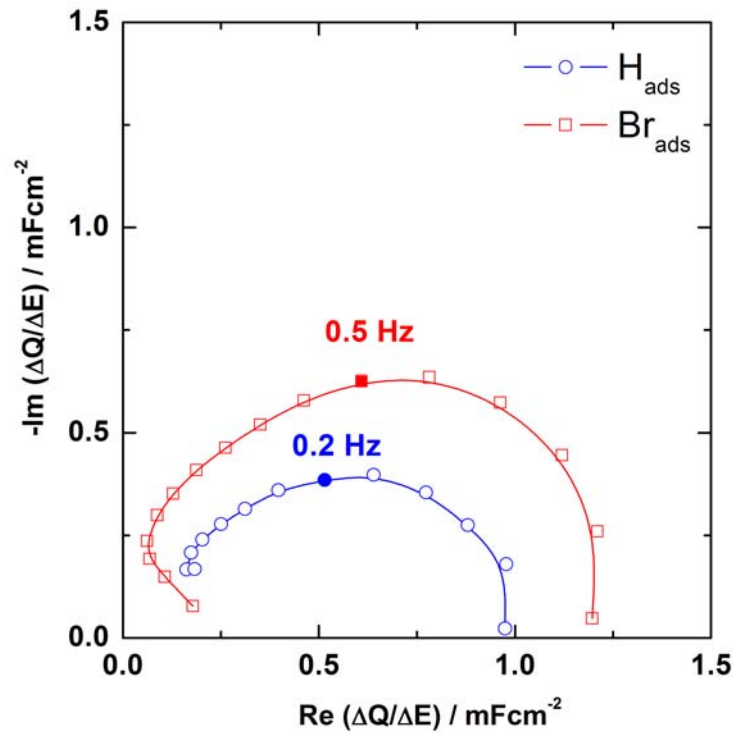
Figure 3



3
4
5

1
2
3

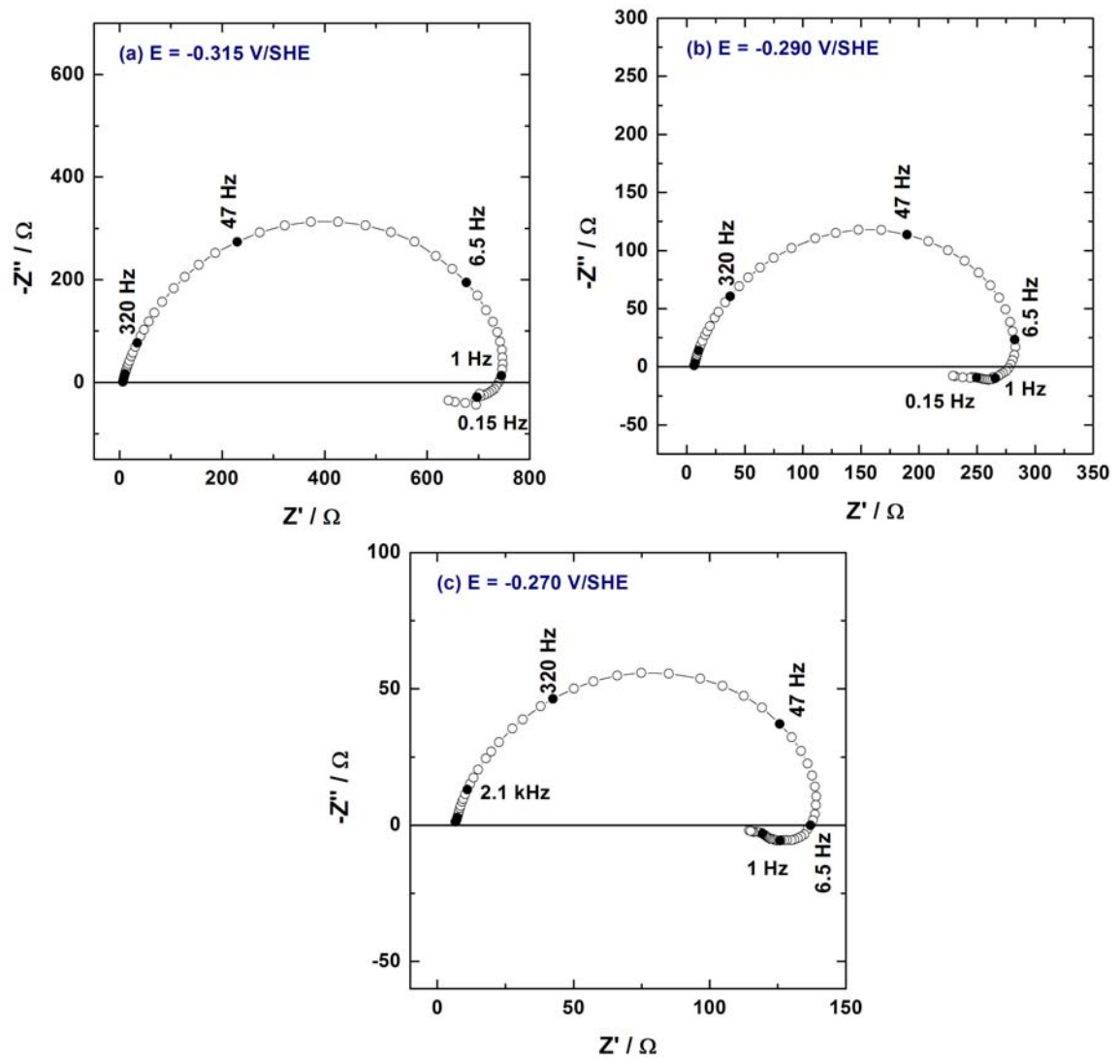
Figure 4



4
5
6

1
2
3

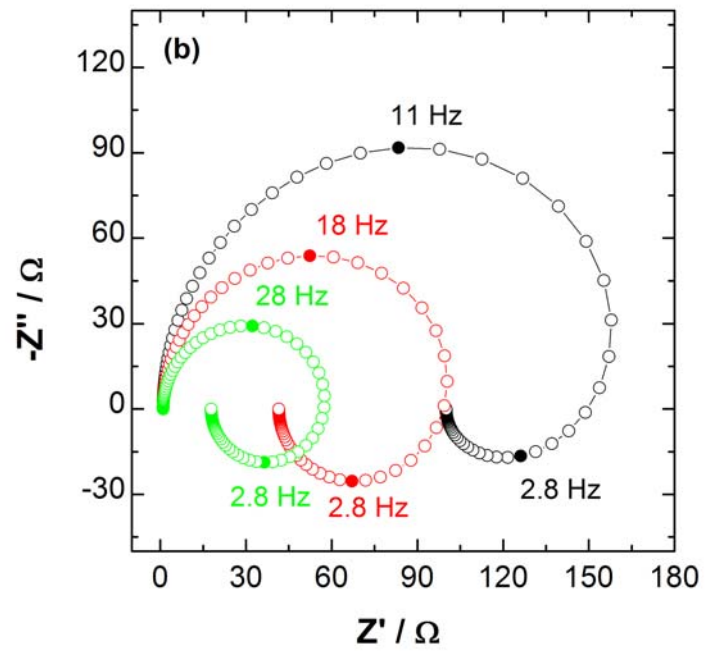
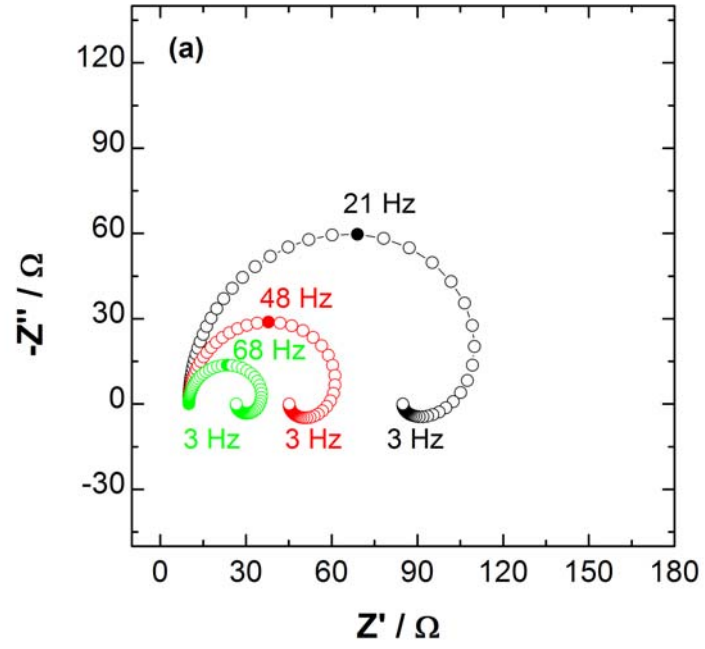
Figure 5



4
5
6
7

1 *Figure 6*

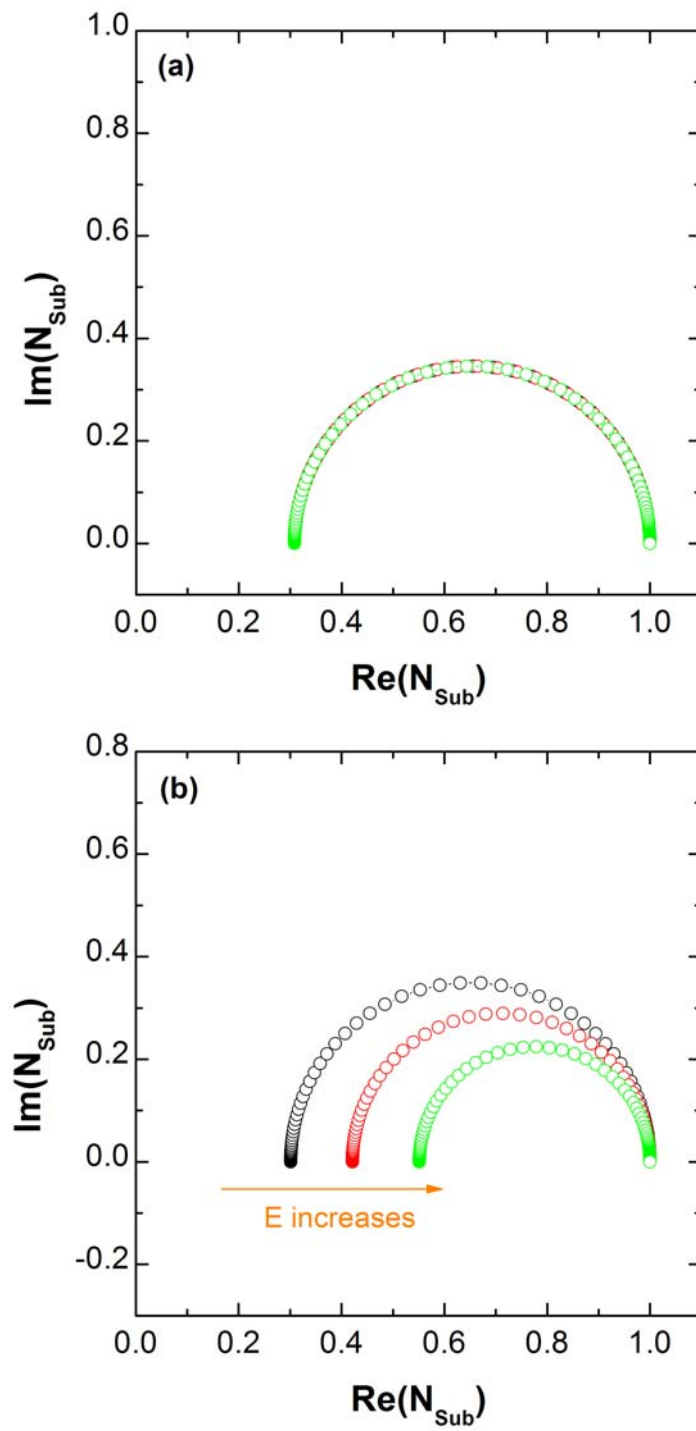
2



3
4

1
2
3

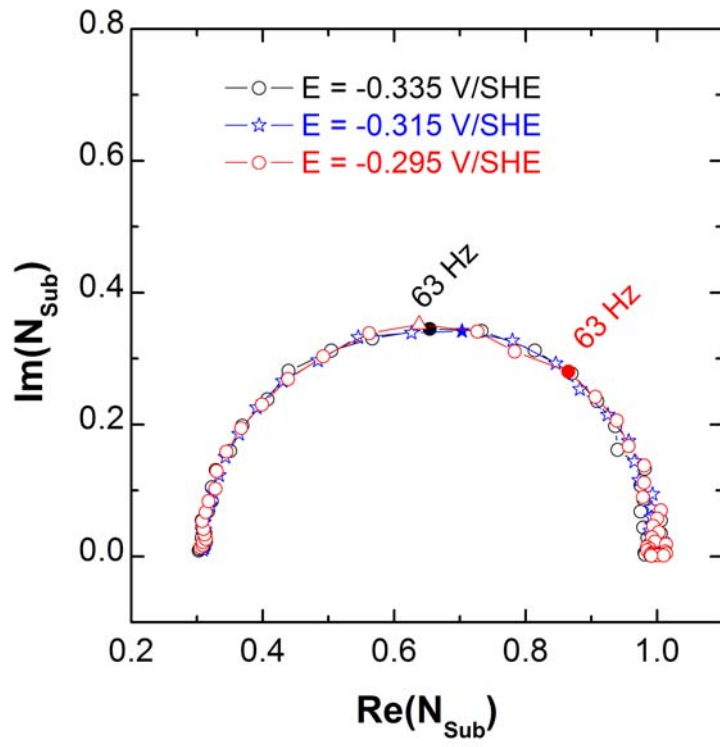
Figure 7



4
5

1 *Figure 8*

2



3
4
5

1
2
3
4

Table 1

	Capacitance / mF cm ⁻²	Charge / μC cm ⁻²	Characteristic Frequency / Hz
Only H _{ads} (without the presence of Br)	3	212	2
H _{ads} competitive with Br _{ads}	1	71	0.2
Br _{ads} competitive with H _{ads}	1.2	85	0.5

5
6
7